Available online at www.sciencedirect.com
SCIENCE DIRECT®
International Journal of Thermal Sciences 42 (2003) 1081–1088
International Journal of Thermal Sciences
www.elsevier.com/locate/ijts

Entropy generation in Poiseuille–Benard channel flow

Hassen Abbassi [a,*], Mourad Magherbi [b], Ammar Ben Brahim [c]

[a] *Faculté des sciences, département de physique, route de Soukra, BP 802, 3018 Sfax, Tunisia*
[b] *Institue préparatoire aux études d'ingénieurs de Gabes, avenue Omar Ibn El Khattab, 6029 Gabes, Tunisia*
[c] *École nationale d'ingénieurs de Gabes, avenue Omar Ibn El Khattab, 6029 Gabes, Tunisia*

Received 26 June 2002; accepted 4 March 2003

Abstract

The issue of entropy generation in Poiseuille–Benard channel flow is analyzed by solving numerically the mass, momentum and energy equations with the use of the classic Boussinesq incompressible approximation. The numerical scheme is based on Control Volume Finite Element Method with the SIMPLER algorithm for pressure–velocity coupling. Results are obtained for Rayleigh numbers *Ra* and irreversibility ϕ ranging from 10^3 to 5×10^4 and from 10^{-4} to 10 respectively. Variations of entropy generation and the Bejan number as a function of *Ra* and ϕ are studied. The limit value ϕ_l for which entropy generation due to heat transfer is equal to entropy due to fluid friction is evaluated. It has been found that ϕ_l is a decreasing function of the Rayleigh number *Ra*. ϕ_l varies from 0.0015 to 0.096 when *Ra* decrease from 5×10^4 to 10^3. Stream lines and entropy generation maps are plotted at six times over one period at $Ra = 10^4$ and $\phi = 10^{-3}$. It has been found that the maximum entropy generation is localized at areas where heat exchanged between the walls and the flow is maximum. No significant entropy production is seen in the main flow.

Keywords: Entropy generation; Irreversible; Periodic; Heat transfer; Convective cell

1. Introduction

Entropy generation has recently been the topic of great interest in many fields such as heat exchangers, turbo machinery, electronic cooling, porous media and combustions. Datta [1] investigated the entropy generation in a confined laminar diffusion flame. He shows that the major contribution to the entropy generation is due to heat transfer within the flame. Baytas [2,3] presented a numerical study on the minimization of entropy generation in an inclined enclosure [2] and inclined porous cavity [3]. The influence of Rayleigh number and inclination angle of the enclosure on entropy generation is evaluated. It has been established that minimum entropy generation depends considerably on Rayleigh number and inclination angle of the enclosure. Sahin [4] studied the entropy generation in a laminar viscous flow through a duct with constant wall temperature. He showed that there could be an optimum size of heat exchanger for which the total irreversibility due to heat transfer and pressure drop becomes minimum. Demirel and Kahraman [5] studied the entropy generation in a rectangular packed duct with wall heat flux. They showed that the irreversibility distribution is not continuous through the wall and core regions. Sahin [6] analytically investigated entropy generation in turbulent liquid flow through a smooth duct subjected to constant wall temperature. It was found that constant viscosity assumption may yield to a considerable amount of deviation on entropy generation. Entropy generation and Lyapunov instability at the onset of turbulent convection were investigated by Castillo and Hoover [7]. They showed that the two flow morphologies at the same Rayleigh number have different rates of entropy generation and different Lyapunov exponent. The harmonic flow produces entropy at greater rate whereas the chaotic flow has a larger maximum Lyapunov exponent. In a recent paper, Narusawa [8] examined the rate of entropy generation both theoretically and numerically for forced and mixed convection in rectangular duct heated at the bottom. In the theoretical study, he expressed the rate of entropy generation as a function of relevant non-dimensional thermal and hydrodynamic fields as well as interaction between the two fields. Effects of the aspect ration of the channel section on the flow

* Corresponding author.
E-mail addresses: hassen.abbassi@fss.rnu.tn (H. Abbassi), ammar.benbrahim@enig.rnu.tn (A. Ben Brahim).

1290-0729/$ – see front matter
doi:10.1016/S1290-0729(03)00095-4

Nomenclature

Be	Bejan number
C_P	specific heat at constant pressure .. $m^2{\cdot}s^{-2}{\cdot}K^{-1}$
g	gravitational acceleration ..... $m{\cdot}s^{-2}$
H	channel width ..... m
k	thermal conductivity of the fluid ..... $kg{\cdot}m{\cdot}s^{-3}{\cdot}K^{-1}$
L	length of the channel ..... m
Nu	local Nusselt number, $= \lvert\partial\theta/\partial y\rvert_w$
Nub	local Nusselt number at the bottom wall
Nut	local Nusselt number at the top wall
$\overline{Nu}$	space averaged Nusselt number
$\langle\overline{Nu}\rangle$	space and time-averaged Nusselt number
P	Pressure nondimensionalized by ρu_{av}^2
Pe	Peclet number, $= Re\,Pr$
Pr	Prandtl number, $= \mu C_P/k$
Ra	Rayleigh number, $= \rho^2 g\beta C_P(T_h - T_c)H^3/\mu k$
Re	Reynolds number, $= u_{av}H/\nu$
s	Entropy generation per unit volume ..... $J{\cdot}m^{-3}{\cdot}s^{-1}{\cdot}K^{-1}$
S	Entropy generation over the entire domain ..... $J{\cdot}s^{-1}{\cdot}K^{-1}$
$\langle S\rangle$	time averaged total entropy generation ..... $J{\cdot}s^{-1}{\cdot}K^{-1}$
T	dimensional temperature ..... K
To	Bulk temperature, $= (T_h + T_c)/2$ ..... K
u_{av}	average *u*-component at the channel inlet $m{\cdot}s^{-1}$
U	velocity vector nondimensionalized by u_{av}
u, *v*	velocity components nondimensionalized by u_{av}
x, *y*	Cartesian coordinates nondimensionalized by *H*

Greek symbols

β	thermal expansion coefficient ..... K^{-1}
θ	dimensionless temperature, $= (T - T_c)/(T_h - T_c)$
Θ	dimensionless period
ϕ	irreversibility distribution ratio
μ	dynamic viscosity of the fluid ..... $kg{\cdot}m^{-1}{\cdot}s^{-1}$
ν	kinematic viscosity of the fluid ..... $m^2{\cdot}s^{-1}$
ρ	density of the fluid ..... $kg{\cdot}m^{-3}$
τ	time nondimensionalized by, $= u_{av}/H$

Subscripts

c	cold
h	hot
av	average
w	wall
l	limit

structure and the rate of entropy generation is the subject of the numerical investigation of Narusawa [8]. He showed that the transition between two and four rolls occurs at the aspect ratio 3.02 and 2.95 for Rayleigh number 2427 and 3777, respectively. The transition of $Ra = 2427$ is accompanied by a clear discontinuity of the entropy generation whereas for $Ra = 3777$, the transition occurs without any discontinuity.

The performance of an engineering system is degraded by the presence of irreversibilities. Entropy generation is a measure of the magnitude of these irreversibilities present during any process. The optimization of thermal devices is then obtained by the minimization of entropy generation. Usually, the optimization is made via parametrical study of the angle of inclination and/or geometrical parameters of the system. This optimization can not be achieved in our case because the Poiseulle–Benard channel flow is standard in inclination (horizontal) and in geometry (two parallel walls). For this reason, the optimization of entropy generation is out of study in this article.

The present paper reports a numerical study of entropy generation in the Poiseulle–Benard channel flow. The investigation is carried out from the numerical solutions of complete Navier–Stokes and energy equations by Control Volume Finite Element Method. During this study, Reynolds and Peclet numbers are fixed at $Re = 10$ and $Pe = 20/3$ whereas Rayleigh number *Ra* and irreversibility ϕ are varied from 10^3 to 5×10^4 and from 10^{-4} to 10 respectively. The Poiseuille–Benard channel flow is usually used for code validation at $Re = 10$, $Pe = 20/3$ and $Ra = 10^4$. Its open boundary conditions complicated by the exit of convective rolls constitute a severe test for numerical codes in computational fluid mechanics. Usually, stream lines, Nusselt number and period of oscillations are determined and compared with available published solutions. In this study we add to the literature of this flow the entropy generation, irreversibility distribution ratio and the Bejan number.

2. Poiseuille–Benard channel flow and boundary conditions

The system of interest is a horizontal plane channel under a vertical temperature gradient as indicated in Fig. 1. Since the Reynolds number is fixed at a weak value ($Re = 10$), under moderate to high values of Rayleigh numbers, convective

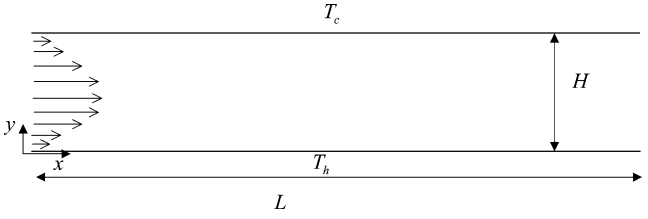

Fig. 1. Model of Poiseuille–Benard channel flow.

rolls appear in the channel alternatively near the lower and the upper walls. This flow is known as Poiseuille–Benard flow. This channel flow indicated in Fig. 1 would be a simple Poiseuille flow if there were no heating or cooling from below and Benard flow if the ends were closed. The flow is supposed to be laminar and two-dimensional.

At the channel inlet, the normal component of velocity is assumed to be zero, and a fully developed parabolic profile for the axial velocity is deployed. No-slip boundary conditions for velocities on all solid walls are used. To avoid discontinuity, the temperature of incoming stream is assumed to vary linearly from T_h at the bottom wall to T_c at the upper wall.

One of the major difficulties encountered in numerical procedure in fluid mechanics is the outflow boundaries. This difficulty arises because the computational domain is bounded whereas the physical domain is unbounded. Then an artificial Open Boundary Condition (OBC) is imposed. With well-posed OBC there is no necessity to have a very large computational domain, whereas incorrect formulation of OBC might propagate to the internal domain and leads to unrealistic results.

The two most popular OBC are the Neumann Boundary Condition (NBC) and the Convective Boundary Condition (CBC) [9] formulated respectively as follow:

$$\frac{\partial \varphi}{\partial x} = 0$$

$$\frac{\partial \varphi}{\partial t} + u_n \frac{\partial \varphi}{\partial x} = 0$$

Where u_n is usually some normal average velocity and φ represents the dependent variable. In their recent study of a flow around a square cylinders in a plane channel, Sohankar et al. [10] concludes that the CBC (compared to NBC) is more effective in reducing the CPU time, reducing the upstream influence of the outlet and then reducing the necessary downstream extent of the domain. Comini et al. [11] obtained very accurate results by employing CBC in the streamfunction–vorticity formulation applied to the benchmark problem of the flow at low Reynolds number in a plane channel heated from below. Detailed investigation in a recent study of Abbassi et al. [12] shows that CBC has a clear superiority to predict the out flow compared to NBC. CBC allows vortices to smoothly pass away from the computational domain then, minimize the distortion of the vortices and reduce perturbations that reflect back into the domain. In the following study the CBC is used in all numerical computations for all dependent variables, and then large extension of the channel is not necessary. Consequently, the aspect ratio is fixed at only $L/H = 5$. Nicolas et al. [13] showed that this value of aspect ratio is sufficient for a numerical study of Poiseuille–Benard channel flow with the use of CBC.

Boundary conditions expressed in dimensionless form are as follows:

$0 \leqslant x \leqslant L/H;\ y = 0\text{: } u = v = 0,\ \theta = 1$

$0 \leqslant x \leqslant L/H;\ y = 1\text{: } u = v = 0,\ \theta = 0$

$x = 0;\ 0 \leqslant y \leqslant 1\text{: } u = 6y(1-y),\ v = 0,\ \theta = 1 - y$

$$x = L/H;\ 0 \leqslant y \leqslant 1\text{: } \frac{\partial \varphi}{\partial \tau} + \frac{\partial \varphi}{\partial x} = 0;\ \int_0^1 u \,\mathrm{d}y = 1$$

3. Governing equations

Equations are formulated considering the usual hypotheses of a Newtonian incompressible fluid and the Boussinesq approximation is assumed to be valid. In the Cartesian coordinate system, the dimensionless equations for continuity, momentum, and energy may be expressed in the following conservative form:

$$\operatorname{div}(\boldsymbol{U}) = 0 \tag{1}$$

$$\frac{\partial u}{\partial \tau} + \operatorname{div}(\boldsymbol{Ju}) = -\frac{\partial P}{\partial x}$$

$$\text{where } \boldsymbol{Ju} = u\boldsymbol{U} - \frac{1}{Re}\,\mathbf{grad}(u) \tag{2}$$

$$\frac{\partial v}{\partial \tau} + \operatorname{div}(\boldsymbol{Jv}) = -\frac{\partial P}{\partial y} + \frac{Ra}{Re \cdot Pe}\theta$$

$$\text{where } \boldsymbol{Jv} = v\boldsymbol{U} - \frac{1}{Re}\,\mathbf{grad}(v) \tag{3}$$

$$\frac{\partial \theta}{\partial \tau} + \operatorname{div}(\boldsymbol{J}\theta) = 0$$

$$\text{where } \boldsymbol{J}\theta = \theta\boldsymbol{U} - \frac{1}{Pe}\,\mathbf{grad}(\theta) \tag{4}$$

In the above equations the space coordinates, velocities, time and pressure are normalized with respectively the width H of the channel, the averaged velocity at the channel inlet u_{av}, the characteristic time H/u_{av}, and the characteristic pressure ρu_{av}^2. The dimensionless temperature $\theta = (T - T_c)/(T_h - T_c)$ is referred to suitably defined "hot" and "cold" temperatures.

The thermal heat flux exchanged between the walls and the flow is characterized by the space-averaged Nusselt number evaluated as follows:

$$\overline{Nu} = \frac{1}{L/B}\int_0^{L/B} Nu \,\mathrm{d}x \tag{5}$$

Where Nu is the local Nusselt number defined as:

$$Nu = \left|\frac{\partial \theta}{\partial y}\right|_w$$

The space- and time-averaged Nusselt number is defined as:

$$\langle \overline{Nu} \rangle = \frac{1}{\Theta}\int_0^{\Theta} \overline{Nu} \,\mathrm{d}\tau \tag{6}$$

Where Θ is the period of oscillations of the space-averaged Nusselt number $\overline{Nu}$.

The non-equilibrium of the flow imposed by boundary conditions causes a continuous entropy generation in the flow field. This entropy generation is due to the irreversible nature of heat transfer and viscosity effects. From the known scalar fields of temperature and velocity components, dimensionless local volumetric entropy generation can be expressed in the Cartesian coordinate system of Fig. 1 as [2]:

$$s = s_{\text{heat transfer}} + s_{\text{fluid friction}} \tag{7}$$

Where:

$$s_{\text{heat transfer}} = \left(\frac{\partial\theta}{\partial x}\right)^2 + \left(\frac{\partial\theta}{\partial y}\right)^2$$

$$s_{\text{fluid friction}} = \phi\left(2\left[\left(\frac{\partial u}{\partial x}\right)^2 + \left(\frac{\partial u}{\partial y}\right)^2\right] + \left(\frac{\partial v}{\partial x} + \frac{\partial u}{\partial y}\right)^2\right)$$

ϕ is irreversibility distribution ratio:

$$\phi = \frac{\mu To}{k}\left(\frac{u_{\text{av}}}{\Delta T}\right)^2$$

The first term on the right-hand side of Eq. (7) shows the local entropy generation due to heat transfer, while the second term shows the local entropy generation due to fluid friction. The dimensionless total entropy generation for the entire channel is obtained by integrating Eq. (7):

$$S = \int_0^1 \int_0^{L/H} s \,\mathrm{d}x \,\mathrm{d}y \tag{8}$$

To the second law of thermodynamic, processes can occur in a certain direction only, for which $S \geqslant 0$. Entropy generation S is greater than zero and equal to zero for irreversible (real) and reversible (ideal) process, respectively. For S less than zero the process is impossible.

The time-averaged total entropy generation is defined as:

$$\langle S\rangle = \frac{1}{\Theta}\int_0^{\Theta} S \,\mathrm{d}\tau \tag{9}$$

The Bejan number Be which compare the magnitude of entropy generation due to heat transfer to the magnitude of the total entropy generation is defined by:

$$Be = \frac{\langle S_{\text{heat transfer}}\rangle}{\langle S\rangle} \tag{10}$$

When $Be \gg 1/2$, the irreversibility due to heat transfer dominates, while for $Be \ll 1/2$ the irreversibility due to viscous effects dominates. For $Be \cong 1/2$, entropy generation due to heat transfer is almost of the same magnitude as that due to fluid friction.

4. Numerical procedure

A modified version of Control Volume Finite-Element Method (CVFEM) of Saabas and Baliga [14] is adapted to the standard staggered grid in which pressure and velocity components are stored at different points. The SIMPLER algorithm was applied to resolve the pressure–velocity coupling in conjunction with an Alternating Direction Implicit (ADI) scheme for performing the time evolution. The numerical code used here is described and validated in details in Abbassi et al. [15,16]. From the known temperature and velocity fields at any instant τ given by solving equations (1)–(4), the local entropy generation s is evaluated at any node of the domain by Eq. (7). The dimensionless total entropy generation for the entire channel S is easily obtained by Eq. (8). The evolution of S for many periods permits the evaluation of the time averaged entropy generation $\langle S\rangle$ by using Eq. (9). From the known temperature gradient at the walls of the channel at any instant, local, space-averaged and time-space-averaged Nusselt numbers are easily evaluated.

5. Results and discussion

The time averaged entropy generation $\langle S\rangle$ is a function of temperature and velocity gradients in the x and y directions in all the calculation domain. $\langle S\rangle$ is then a good indicator of grid dependence. Grid refinement tests have been performed for the case $Re = 10$, $Pe = 20/3$ and $Ra = 10^4$ using three uniform grids 70×20, 101×26 and 131×31. Results show that when we pass from a grid of 70×20 to a grid of 101×26 time-averaged entropy generation $\langle S\rangle$ undergoes an increase of 7.1%. When we pass from the grid of 101×26 to the grid of 131×31, $\langle S\rangle$ undergoes an increase of only 1.6%. We conclude that the grid 101×26 is sufficient to carry out a numerical study of this flow. This grid is retained for all following investigations.

Fig. 2 presents the evolution of stream lines and entropy generation maps over one period at $Ra = 10^4$ and $\phi = 10^{-3}$. Images are taken at time intervals of $\Theta/6$, where Θ is the dimensionless period equal to 2.63. The starting time $\tau = 0$ for these images is the instant when the averaged Nusselt number at the bottom wall $\overline{Nub}$ is maximum. This instant is chosen arbitrary. As shown in Fig. 2, convective cells appear in alternation near the bottom and the top walls moving in the direction of the main flow as cylinders turning without translation on walls. Cells on the bottom are turning in the clockwise sense whereas cells on the top wall are turning in the anticlockwise sense. The existence of convective cells imposes the formation of Von Karmann street centered at the channel axes. The waved structure of the flow imposes to scalar quantities such as temperature and velocity components to be periodic. At all instants, maps shows that entropy generation S is maximum in some surfaces alternatively shared near the two walls. No significant entropy production is seen in the main flow. Regions of maximum entropy are located at the right and left sides of lower and upper cells respectively. Why does entropy S is maximum in these locations? The answer is found in Fig. 3 where we plot the variation of the

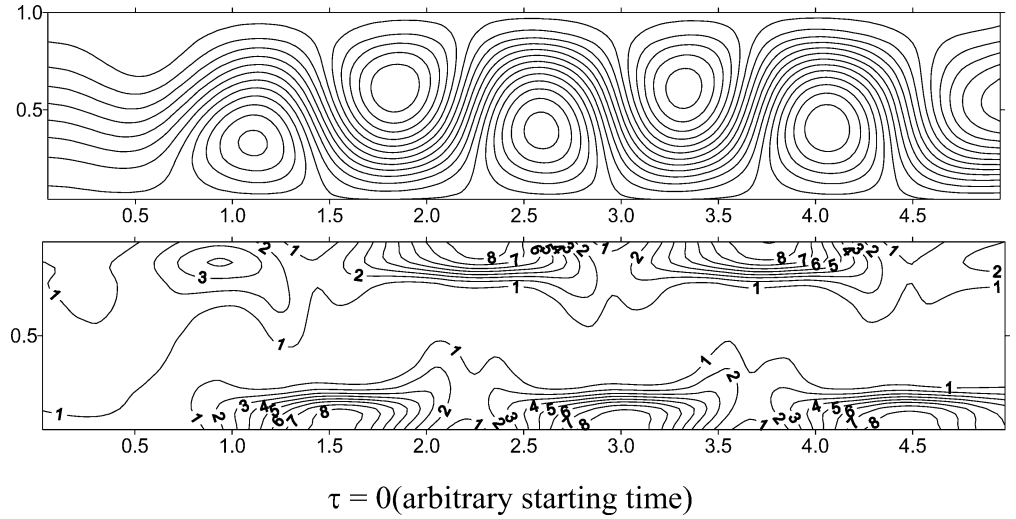

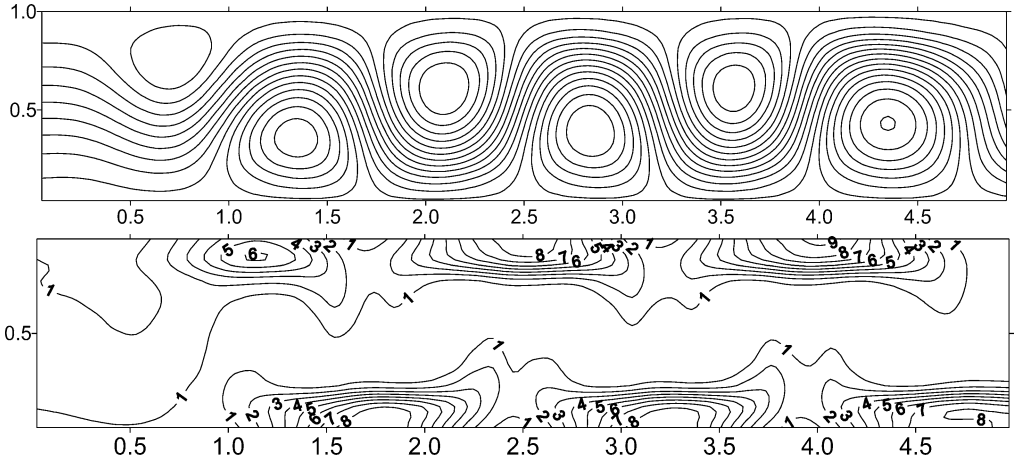

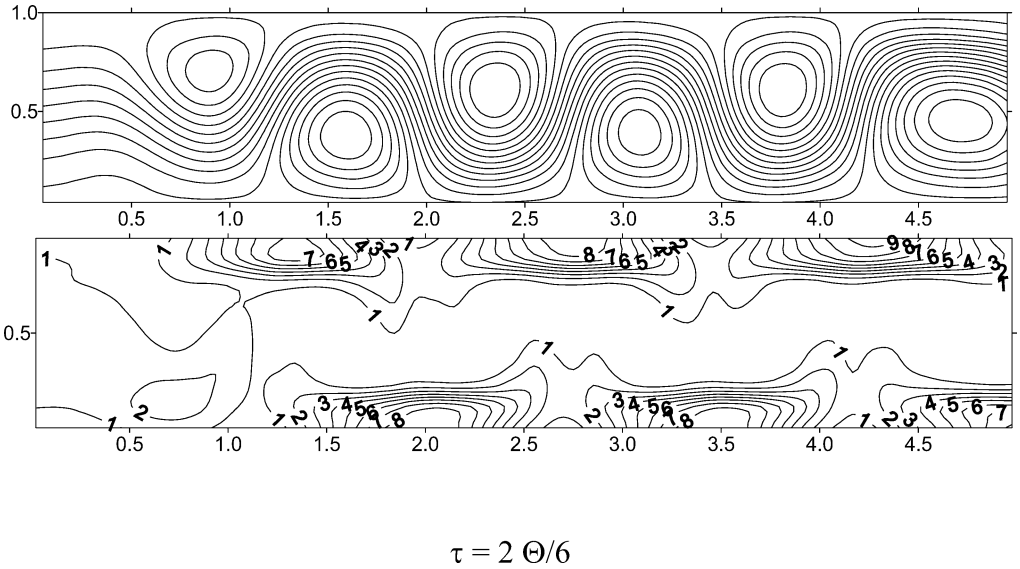

Fig. 2. Evolution during one period of respectively stream lines and entropy generation maps at $Ra = 10^4$ and $\phi = 10^{-3}$.

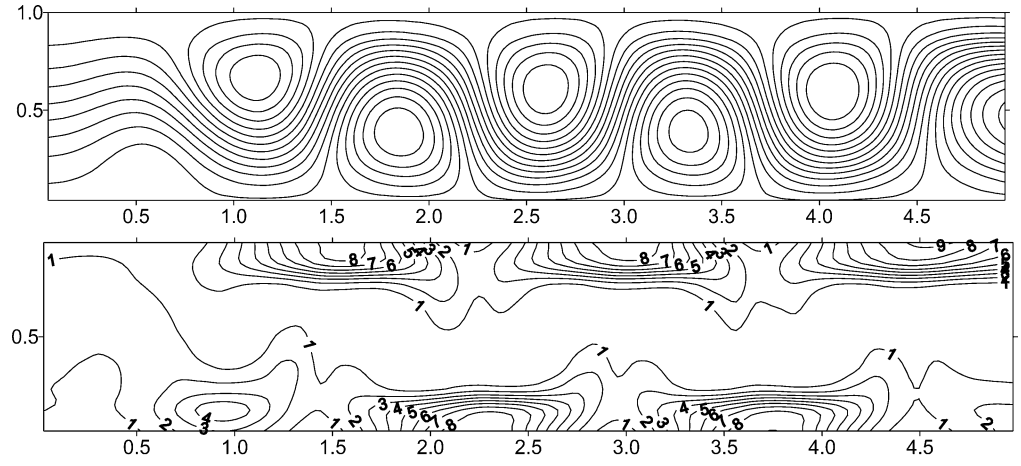

$\tau = 3\ \Theta/6$

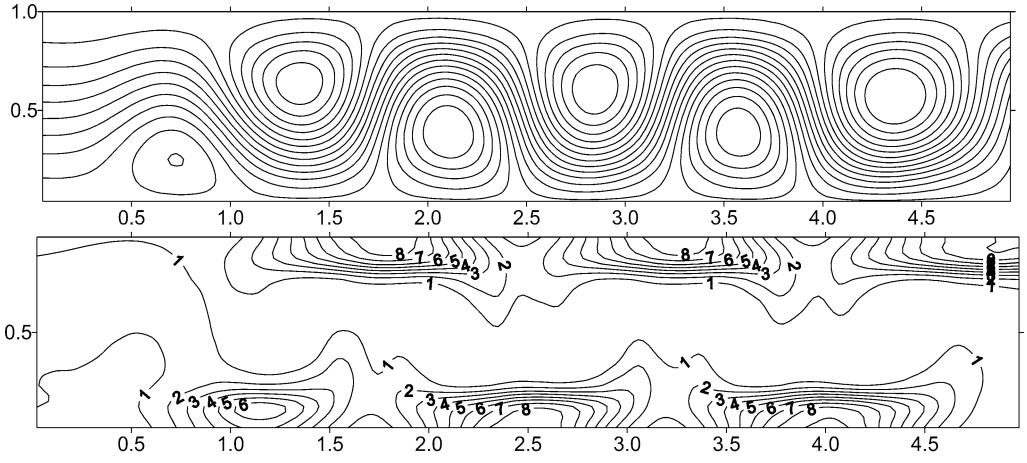

$\tau = 4\ \Theta/6$

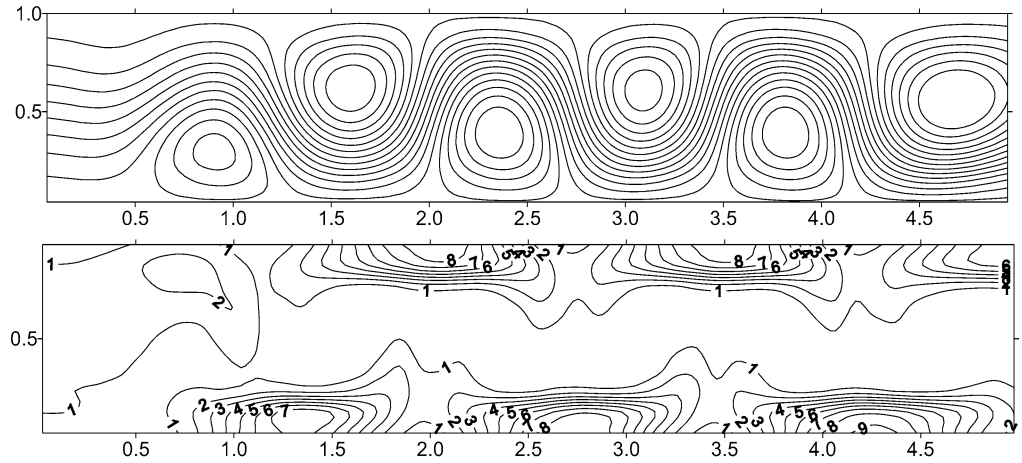

$\tau = 5\ \Theta/6$

Fig. 2. (Continued).

local Nusselt numbers *Nub* and *Nut* along bottom and top walls respectively at same instant corresponding to the first figure of stream lines. We remark easily that regions of maximum entropy generation coincides exactly with regions of maximum Nusselt numbers. We can conclude that augmentation of energy exchanged between the flow and the

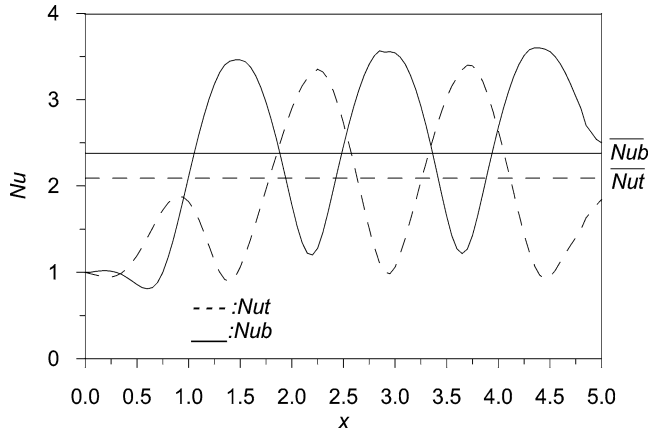

Fig. 3. Local Nusselt numbers *Nub* and *Nut* respectively along the bottom and the top walls at the arbitrary starting time $\tau = 0$ of Fig. 2. $Ra = 10^4$.

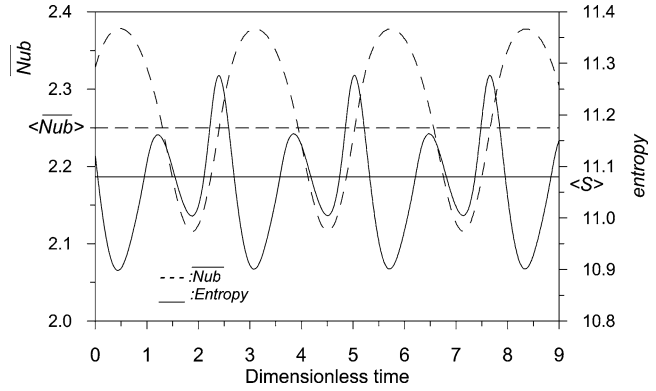

Fig. 4. Evolutions of the space averaged Nusselt number of the bottom wall and the entropy generation S at $Ra = 10^4$ and $\phi = 10^{-3}$.

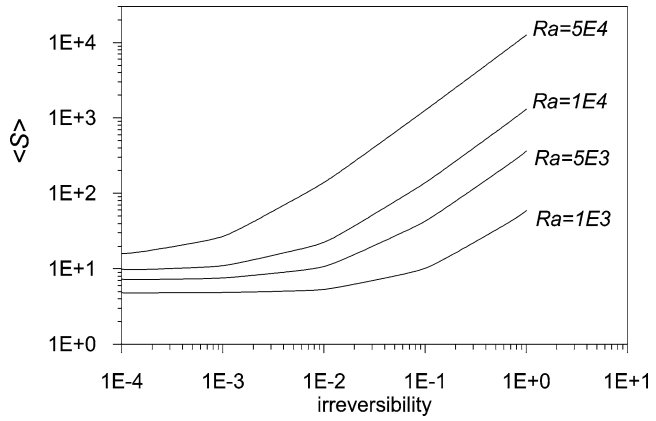

Fig. 5. Time averaged entropy generation versus irreversibility.

walls contribute to an augmentation of entropy generation via the augmentation of temperature gradient near the walls. It should be noted that averaged Nusselt numbers $\overline{Nub}$ and $\overline{Nut}$ have a periodic evolution. They are oscillating in opposing phases with the same period than the flow. For this reason, in Fig. 3 we see $\overline{Nub}$ different than $\overline{Nut}$.

Fig. 4 is a plot of the evolutions of the space averaged Nusselt number at the bottom wall $\overline{Nub}$ and the global entropy generation S at $Ra = 10^4$ and $\phi = 10^{-3}$. $\overline{Nub}$ which

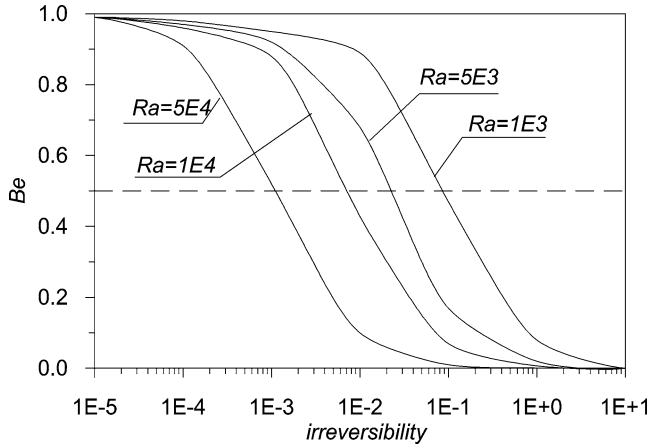

Fig. 6. Bejan number versus irreversibility.

characterize the heat transferred from the bottom wall to the flow and determined by the use of only temperature gradient, is perfectly sinusoidal around the value $\langle\overline{Nub}\rangle = 2.25$ with dimensionless period $\Theta = 2.63$. The evolution of the global entropy generation S is harmonic but not sinusoidal; it has two maximums and two minimums, both absolute and relative extremes are oscillating around $\langle S\rangle = 11.08$. This is due to the fact that S is the sum of many temperature and velocity gradients. These gradients are not necessary of the same phase and amplitude, their sum has lead to the harmonic signal indicated in Fig. 4. The period of S is the same than $\overline{Nub}$.

The variation of the time averaged entropy generation $\langle S\rangle$ as a function of the irreversibility ϕ is plotted in Fig. 5. For a fixed Rayleigh number, then for a fixed temperature difference $\Delta T = T_h - T_c$, $\langle S\rangle$ is an increasing function of the irreversibility ϕ , then an increasing function of the bulk temperature $To = (T_h + T_c)/2$. The increase of $\langle S\rangle$ is slow for weak values of ϕ and becomes quick for high values of ϕ. For a given irreversibility value, $\langle S\rangle$ is also an increasing function of the Rayleigh number.

The objective of Fig. 6 is the determination of the limit value of the irreversibility noted ϕ_l verifying $Be = 1/2$ for different Rayleigh numbers. As we noted earlier, the Bejan number compares the entropy generation due to heat transfer to the global entropy generation. For Rayleigh numbers equal to 5×10^4, 10^4, 5×10^3 and 10^3 the limit values ϕ_l of the irreversibility is found respectively equal to 0.0015, 0.0066, 0.04 and 0.096. For a given Rayleigh number, if ϕ is less than ϕ_l, entropy generation due to heat transfer is more intense than entropy due to fluid friction.

6. Conclusion

The distribution of entropy generation in 2D laminar Poiseuille–Benard channel flow has been studied numerically from direct solutions of complete Navier–Stokes and energy equations. Reynolds and Peclet numbers were fixed at $Re = 10$ and $Pe = 20/3$ whereas Rayleigh number *Ra* and

irreversibility ϕ are varied from 10^3 to 5×10^4 and from 10^{-4} to 10, respectively. Based on the calculated results, the following conclusion can be drown.

(1) Entropy generation is largely higher near the channel walls than that in the central flow.
(2) Maximum of entropy generation is located just near the walls in the regions where Nusselt number is maximum, i.e., where thermal heat exchanged between the flow and walls is maximum.
(3) For a fixed value of ΔT, the global entropy generation S increase with increasing the bulk temperature To of the channel.
(4) The limit value ϕ_l of the irreversibility corresponding to $Be = 1/2$ increases when the Rayleigh number decrease. For Ra equal to 5×10^4, 10^4, 5×10^3 and 10^3, ϕ_l is respectively equal to 0.0015, 0.0066, 0.04 and 0.096.

References

[1] A. Datta, Entropy generation in a confined laminar diffusion flame, Combust. Sci. Technol. 159 (2000) 39–56.
[2] A.C. Baytas, Optimization in an inclined enclosure for minimum entropy generation in natural convection, J. Non-Equilib. Thermodyn. 22 (1997) 145–155.
[3] A.C. Baytas, Entropy generation for natural convection in an inclined porous cavity, Internat. J. Heat Mass Transfer 43 (2000) 2089–2099.
[4] A.Z. Sahin, Second law analysis of laminar viscous flow through a duct subjected to constant wall temperature, ASME J. Heat Transfer 120 (1998) 76–83.
[5] Y. Demirel, R. Kahraman, Entropy generation in a rectangular packed duct with wall heat flux, Internat. J. Heat Mass Transfer 42 (1999) 2337–2344.
[6] A.Z. Sahin, Entropy generation in a turbulent liquid flow through a smooth duct subjected to constant wall temperature, Internat. J. Heat Mass Transfer 43 (2000) 1469–1478.
[7] V.M. Castello, W.G. Hoover, Entropy production and Lyapunov instability at the onset of turbulent convection, Phys. Rev. E 58 (1998) 7350–7354.
[8] U. Narusawa, The second-law analysis of mixed convection in rectangular ducts, Heat Mass Transfer 37 (2001) 197–203.
[9] R.L. Sani, P.M. Gresho, Résumé and remarks on the open boundary condition minisymposium, Internat. J. Numer. Methods Fluids 18 (1994) 983–1008.
[10] A. Sohankar, C. Norberg, L. Davidson, Low-Reynolds-number flow around a square cylinder at incidence: Study of blockage, onset of vortex shedding and outlet boundary condition, Internat. J. Numer. Methods Fluids 26 (1998) 39–56.
[11] G. Comini, M. Manzan, G. Cortella, Open boundary conditions for the stream-function of unsteady laminar convection, Numer. Heat Transfer Part B 31 (1997) 217–234.
[12] H. Abbassi, S. Turki, S. Ben Nasrallah, Channel flow past bluff-body: Outlet boundary condition, vortex shedding and effects of buoyancy, Comput. Mech. 28 (1) (2002) 10–16.
[13] X. Nicolas, P. Traore, A. Mojtabi, J.P. Caltagirone, Augmented Lagrangian method and open boundary conditions in 2D simulation of Poiseuille–Benard channel flow, Internat. J. Numer. Methods Fluids 25 (1997) 265–283.
[14] H.J. Saabas, B.R. Baliga, Co-located equal-order control-volume finite-element method for multidimensional, incompressible, fluid flow, Numer. Heat Transfer B 26 (1994) 381–407.
[15] H. Abbassi, S. Turki, S. Ben Nasrallah, Mixed convection in a plane channel with a built-in triangular prism, Numer. Heat Transfer A 39 (3) (2001) 307–320.
[16] H. Abbassi, S. Turki, S. Ben Nasrallah, Numerical investigation of forced convection in a plane channel with a built-in triangular prism, Internat. J. Thermol. Sci. 40 (2001) 649–658.